agriculture

*Article*

# Parameter Optimization of Reciprocating Cutter for Chinese Little Greens Based on Finite Element Simulation and Experiment

**Wei Wang [1], Xiaolan Lv [2,3] and Zhongyi Yi [2,3,*]**

[1] Key Laboratory of Modern Agricultural Equipment and Technology, Ministry of Education, Jiangsu University, Zhenjiang 212013, China
[2] Institute of Agricultural Facilities and Equipment, Jiangsu Academy of Agricultural Science, Nanjing 210014, China
[3] Key Laboratory for Protected Agricultural Engineering in the Middle and Lower Reaches of Yangtze River of Ministry of Agricultural and Rural Affairs, Nanjing 210014, China
* Correspondence: 20140006@jaas.ac.cn

**Abstract:** Optimizing the working performance of the cutting device for harvesting Chinese little greens is crucial to reducing energy consumption in cutting and improving cutting quality. To explore the mechanical characteristics of leafy vegetables in cutting, the dynamic process of cutting Chinese little greens with a cutter was simulated numerically by using the finite element method based on theoretical analysis. In the numerical simulation, the response-surface methodology (RSM) and central composite rotatable design (CCD) were used to describe the influence rule of sliding–cutting angle ($X_1$), oblique angle ($X_2$), and the average cutting speed ($X_3$) on cutting stress. Then, the stress distribution pattern produced by the cutting blade and the stalks were evaluated by using different working parameters. Subsequently, taking the minimum cutting stress as the target value, the best combination of cutter structure and working parameters were obtained: the sliding–cutting angle was 29°, the oblique angle was 38°, and the average cutting speed was 500 mm/s. At the condition of optimal parameter combinations, the ultimate cutting stress of the upper cutting blade was 0.95 Mpa and that of the bottom cutting blade was 0.77 Mpa. A cutting test was carried out by using a bench test of the cutting performance, and the mechanical properties of cutting at different cutting speeds were studied. Test results showed that at the optimal cutting speed of 500 mm/s, the cutting stress on the cutter was relatively small and the cutting effect reached the best value. The finite element simulation of cutting the little greens reduced the test cost and provided a reference for the development of a cutting device with low power consumption.

**Keywords:** cutting system; numerical simulation; response-surface methodology; parameter optimization; mechanical properties



**Citation:** Wang, W.; Lv, X.; Yi, Z. Parameter Optimization of Reciprocating Cutter for Chinese Little Greens Based on Finite Element Simulation and Experiment. *Agriculture* **2022**, *12*, 2131. https://doi.org/10.3390/agriculture12122131

Academic Editor: Wen-Hao Su

Received: 18 October 2022
Accepted: 6 December 2022
Published: 12 December 2022



## 1. Introduction

Chinese little greens, whose scientific name is non-heading cabbage, are rich in nutrients and are one of the important vegetable varieties in China. With a large planting density and a short growth cycle, Chinese little greens can be harvested 18–25 days after sowing [1]. However, at present, the harvest of Chinese little greens is still completed manually with low harvesting efficiency and high work intensity. Mechanized harvesting operation is the key to solving this problem.

The stress–strain process for cutting failure of the plant stalk fiber layer can be divided into three stages: elastic deformation, plastic deformation, and shear failure. First, the cutter presses the stalk to bend and deform elastically. Then, the cutter continues to bend the stalk to produce plastic deformation and the fiber tensile stress continues to increase. Then, the fibers near the blade break off and eventually fail. Eventually, the entire fiber

layer slips and breaks, causing shear damage to the entire stalk [2]. Studies have found that the mechanical properties during cutting of crop stalks are closely related to the working parameters of the cutting device [3,4].

Relevant scholars studied cutting characteristics using the quasi-static experimental method [5]. Cui et al. [6] designed a shear fixture on a universal materials tester, and selected the blade distance, sliding–cutting angle, skew cutting angle, and shearing angle as test factors to study the shearing characteristics of lettuce stems, and obtained the best cutting combination parameters. Zhang et al. [7] also reported similar results in a shear stress test of a single rice stem, in which the peak cutting force decreased with the sliding–cutting angle. Esgici et al. [8] used a material testing machine to study the influence of grapevine diameter and age on the cutting force, and found that the cutting force was proportional to the vine diameter and age. Du et al. [9] established a mechanical model of the cabbage cutting process, and studied the influence of sliding–cutting angle and cutting speed on fracture, and verified and analyzed it through experimental data. In a study of cutting red bean stalks, the shear stress generated by the 28° bevel angle was smaller than that generated by the 0° bevel [10]. Clementson and Hansen [11] showed that the cutting force of the machete is smaller than that of the chopper in sugarcane harvesting. However, the quasi-static experimental method cannot fully reflect the cutting characteristics of crop stalks, and the influence factors such as the motion parameters of the cutting blade are ignored.

To simulate the actual operation mode of the cutting process, scholars have analyzed the effect of cutting and feeding speed on the cutting characteristics by developing a stalk-cutting test bench [12–14]. Johnson et al. [15] conducted an in-depth study on the cutting energy of the cutting tool under different working parameters and found that the cutting energy of miscanthus stalk was proportional to the cutting speed. Mathanker et al. [16] used the same equipment to evaluate the effect of cutting speed and blade bevel on cutting energy, and found that the specific cutting energy increased with the increasing cutting speed. The research of Allameh and Alizadeh found that the cutting speed of the shear parts had a significant impact on cutting energy. When the cutting speed increased from 1.5 to 2.5 m/s, the cutting energy grew by 77%. At the same time, the interaction between the cutting angle and the bevel angle had a significant impact on the cutting energy [17]. Zhao et al. [18] selected the blade angle, blade shape, cutting speed, and cutting angle as the test factors and studied the effects of working parameters on power consumption by means of mathematical statistics on a self-designed testing system, and obtained the optimal parameter combination for cutting performance of maize stalks under no-support cutting status.

In general, the cutting process of plant stalks belongs to the category of typical high-speed collision and penetration. The contact process between the cutting blade and the stalk forms a randomly nonlinear interaction relationship; hence, it is difficult for traditional physical methods to analyze the cutting mechanism between them. At present, numerical simulation technology has become one of the important tools for solving engineering practice problems [19]. The dynamic simulation analysis can efficiently simulate the non-linear dynamic contact conditions in stalk cutting, and visualize the force and deformation conditions during the cutting process. Meng et al. [20] established a simulation model and studied the influence of working conditions of the circular cutter to determine the best cutting parameters. Yang et al. [21] established an analytical three-dimensional model of the cutting system by using the ANSYS/LS-DYNA software f, and provided a reference for the optimization of the cutter's parameters and the cutting method. Huang et al. [22] studied the dynamic characteristics of the reciprocating cutting system, and evaluated the dynamic response of the cutting system by factors such as cutting speed and inclination angle by numerical simulation and cutting experiments. Qiu et al. [23] found that numerical simulation technology could accurately simulate the cutting process of sugarcane stalks, and analyzed the influence of external and internal factors in the cutting process on the cutting quality, and finally determined the best working parameters based on the simulation

results and orthogonal experiments. In summary, although most of the existing studies on numerical simulation of the cutting process of plant stems are focused on the cutting method of a circular saw blade, it shows that using computer technology can effectively solve stem-cutting problems.

Research on crop stalk-cutting devices has matured, but related research is mainly concentrated on sugarcane, hemp, miscanthus, and other crops. Therefore, it is necessary to study the structural and working parameters of the cutting devices that specially match with the mechanized harvesting of Chinese little greens.

## 2. Materials and Methods

### *2.1. Experiment Influencing Factors and Evaluation Indexes*

During the cutting process, the cutter continues to be subjected to nonlinear force from the plant stalk until the stalk is cut off. The force for cutting plant stalks is the cutting force, which is closely related to cutting energy consumption. Large cutting resistance will inevitably cause greater power consumption in cutting. Therefore, the cutting stress on the cutter is selected as the evaluation index for cutting power consumption and cutting quality [24,25].

The reciprocating cutting system of the cutting machine includes a drive motor, an underdriving gear set, an eccentric wheel mechanism, a blade holder, and a cutting blade [14]. The reciprocating cutting blade is driven by an eccentric cam mechanism to create a reciprocating linear movement with fast cutting frequency and excellent dynamic balance ability while it is working. Its structure is shown in Figure 1.

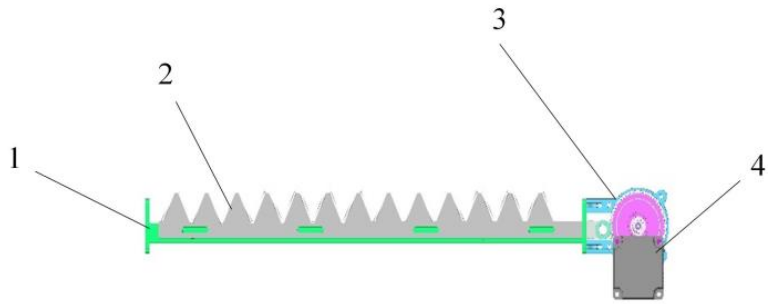


**Figure 1.** The structure drawing of the reciprocating cutter system: 1—cutter holder; 2—cutter; 3—transmission mechanism; 4—motor.

In order to facilitate the theoretical analysis of the cutting process, it is assumed that the stalk is a homogeneous body, and the cutting blade is always in the same plane during the cutting process, regardless of the vibration during the cutting process. When the cutter first contacts the stalk, the stalk deforms elastically at the contact point. Since the absolute speed change is large at this time, the cutting resistance rises rapidly. There is a positive correlation between cutting feed and cutting resistance before reaching the allowable limit. When this limit is exceeded, the stalk undergoes plastic deformation. The length of the line contact between the blade and the stalk continues to change, and the cutting force presents a fluctuating process. At this time, the force of the stalk on the cutter is mainly horizontal cutting force $F_a$, vertical cutting force $F_p$, and inertial force $F_n$. In addition, *V1* and *V2* are the cutting speeds of the upper and lower blades, respectively, and β is the angle of the blade.

In the *XY* plane, the moving direction of the unit cutting force P is the same as the contact point of the cutting blade and the stalk. The movement path of the contact point is a composite of the lateral movement of the cutting blade and the forward movement of the harvesting machine. The cutting resistance on the cutting blade is the integral of the unit cutting force in the contact length between the cutter and the stalk (Figure 2b).

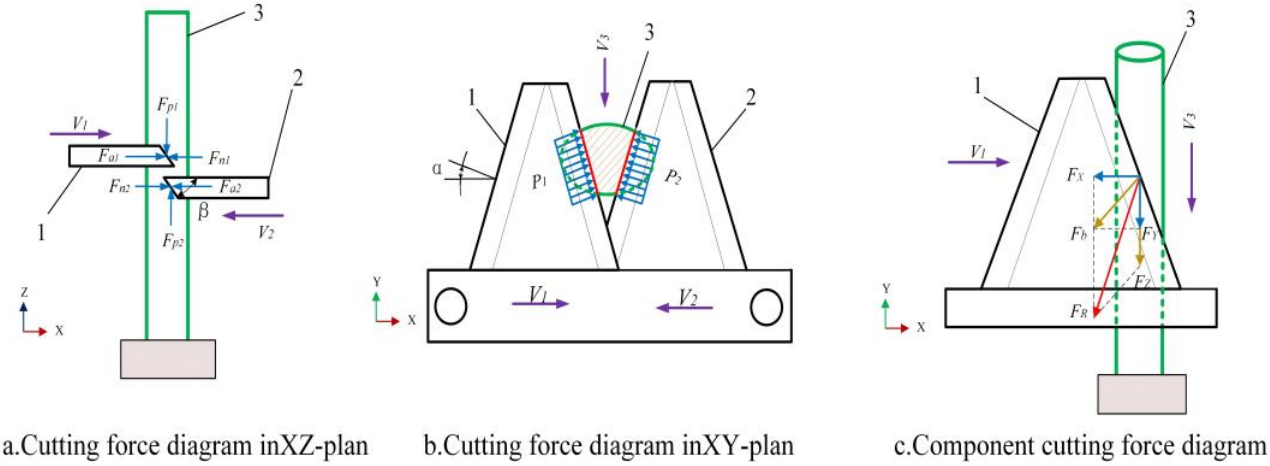


a.Cutting force diagram inXZ-plan b.Cutting force diagram inXY-plan c.Component cutting force diagram

**Figure 2.** Reciprocating cutter-system cutting force diagram: 1—upper cutting blade; 2—bottom cutting blade; 3—stalk.

Therefore, the sliding friction force at the contact point can be decomposed into the component forces in the $X$ and $Y$ directions, and the direction is opposite to the relative movement direction [23]. For convenience in the analysis, the cutting resistance force $F_R$ at the contact point is decomposed into three mutually perpendicular component forces, which are the horizontal force $F_x$ along the cutting direction, the horizontal force $F_y$ along the feed direction, and the force $F_z$ perpendicular to the $XOY$ plane, as shown in Figure 2c. Then, the cutting force $F_R$ is expressed as follows:

$$F_R = \sqrt{F_x^2 + F_y^2 + F_z^2} \tag{1}$$

In this study, the smaller vertical component $F_z$ was ignored, and only the horizontal direction forces $F_x$ and $F_y$ were considered. To avoid the effect of the cutting force that is changed with the stalk diameter of Chinese little greens, according to previous studies, the maximum cutting stress was taken as the evaluation index of the cutting property, and the cutting stress $\sigma$ was calculated by Equation (2) [6]:

$$\sigma = \frac{F_{max}}{A} \tag{2}$$

where the $F_{max}$ is the maximum cutting force in horizontal direction, N; and A is the cross-sectional area of the stalk at the cutting position, $mm^2$.

The factors that affect the shear stress are the structural and movement parameters of the cutter [26–28]. In this study, the three factors, sliding–cutting angle, oblique angle, and average cutting speed, were taken as the factors that affect the cutting mechanical property was analyzed.

### *2.2. Finite Element Modeling and Analysis*

#### 2.2.1. Geometric Model

The three-dimensional geometric model of the reciprocating cutting system unit was established by applying the modeling software SolidWorks. In order to improve the accuracy of the solution and shorten simulation operation time, the cutting system model was appropriately optimized, and a cutting unit was extracted for calculating the simulation when constructing the physical model of the cutting system [23,29]. In Figure 3, the simulation model includes three parts: the upper cutting blade, the bottom cutting blade, and the stalk of Chinese little greens.

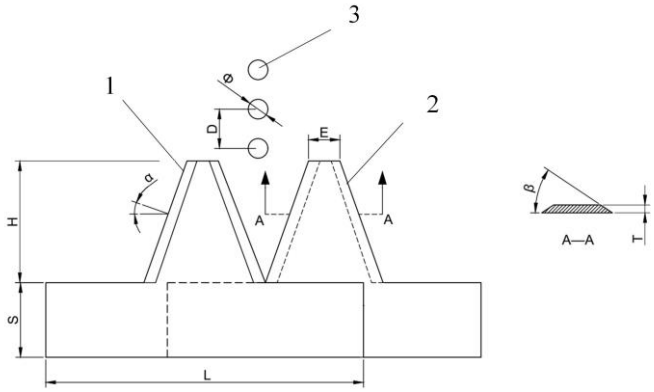


**Figure 3.** The structural diagram of the geometric model: 1—upper cutting blade; 2—bottom cutting blade; 3—stalk.

The cutting blade was regarded as the same integral rigid body, whose features such as the drive motor and transmission components were omitted, but the oblique angle was retained. In the modeling of the greens, it grew with no inclination angle to the ground, and no branches on the stems. The difference between cortex and xylem was ignored. At the same time, each stem to be cut was assumed to be relatively independent, and there was no implicated force between the stems. In addition, the gap between the cutting blade and stem was narrowed as much as possible to reduce the computing time and the amount of calculation. In Table 1, the primary geometric parameters are listed. The three-dimensional geometric model of the reciprocating cutting system unit is shown in Figure 3. The model was saved in Parasolid (*.x_t) format.

**Table 1.** Primary parameters of the geometric model.

| Parameters | Values | Parameters | Values |
|---|---|---|---|
| Tool holder width S/mm | 19 | Cutter top width E/mm | 8 |
| Cutter unit length L/mm | 80 | Cutter thickness T/mm | 2 |
| Cutter edge height H/mm | 31 | Oblique angle β/° | 35, 40, 45 |
| Sliding–cutting angle α/° | 20, 25, 30 | Stalk diameter Φ/mm | 5 |

### 2.2.2. Material Property Parameters

The ANSYS Workbench has a rich database of materials, and structural steel material was selected as the material for the cutter. The cutting process of the stalk is essentially a state of penetration destruction, and large deformation and destruction inevitably occur as the material fails. The model of the stem adopts linear elastic anisotropic material properties; the constitutive parameters of the materials are shown in Table 2 [30].

**Table 2.** Main material parameters of the geometric model.

| Material | Stalk | Blade |
|---|---|---|
| Density ρ/ kg·m$^{-3}$ | 800 | 7850 |
| Young's modulus $E_X$/Mpa | 20.5 | $2.0 \times 10^5$ |
| Young's modulus $E_Y$/Mpa | 20.5 | $2.0 \times 10^5$ |
| Young's modulus $E_Z$/Mpa | 3.5 | $2.0 \times 10^5$ |
| Shear modulus $G_{XY}$/Mpa | 7.88 | $7.7 \times 10^4$ |
| Shear modulus $G_{XZ}$/Mpa | 1.35 | $7.7 \times 10^4$ |
| Shear modulus $G_{YZ}$/Mpa | 1.35 | $7.7 \times 10^4$ |
| Poisson's ratio $\mu_{XY}$ | 0.35 | 0.3 |
| Poisson's ratio $\mu_{XZ}$ | 0.3 | 0.3 |
| Poisson's ratio $\mu_{YZ}$ | 0.3 | 0.3 |

2.2.3. Meshing

The ANSYS Workbench contains multiple built-in meshing methods. In this simulation, a hexahedral meshing method was adopted. In order to ensure the accuracy of the simulation, proper mesh densification was performed on the part where the cutter contacts during meshing [31,32]. The model element size of the cutter and the stalk were both 0.8 mm, and the element size of the dense part of the stalk was 0.6 mm. The total number of elements in the cutting model was 8280 together with 11,842 nodes. The finite element model meshing is shown in Figure 4.

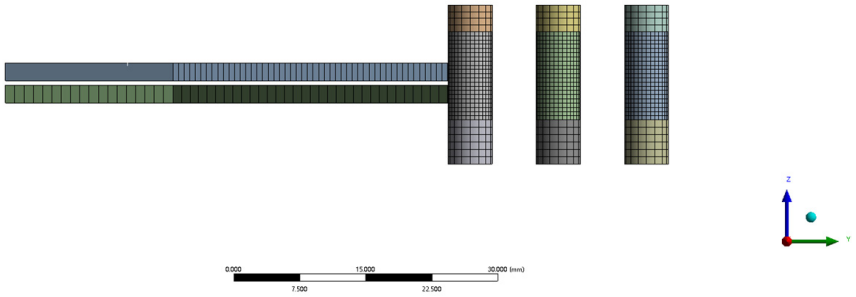


**Figure 4.** The finite element model.

2.2.4. Loads and Constraints

Initial conditions and boundary constraints were determined according to actual working conditions. It was assumed that there was hard soil. The constraint of the ground on the stalks was assumed to be a cantilever beam constraint. The stalks were constrained in the *X* and *Z* directions at its bottom to limit the displacement in both the *X* and *Z* directions. The speed in the *Y* direction was given, and then the same speed of the harvesting machine was simulated. The influence of the mechanical vibration of the cutter during the cutting process was ignored, and it was assumed that the cutting blade always moves in the same plane.

The constraint of the cutting blade was the displacement constraint in the fixed *Y* and *Z* directions; that is, the cutting blade only moves in the opposite direction of the *X* direction, and the speeds of the upper cutter and the bottom cutter were equal in reverse. During the cutting process, the interaction between the cutting blade and the stalk belongs to the category of stab. Hence, the contact type was defined as surface-to-surface erosion contact. The dynamic friction coefficient between the cutter and the stalk was set to 0.38, and the static friction coefficient was set to 0.4 [20].

*2.3. Orthogonal Test Design*

The central–composite test design was adopted [33]. By taking the maximum cutting equivalent stress σ1 of the upper cutting blade and the maximum cutting equivalent stress σ2 of the bottom cutting blade as the target value, then the cutting blade sliding–cutting angle, oblique angle, and the average cutting speed were the three factors used to design an orthogonal test with three factors and five levels. The sliding–cutting angle is an important parameter that affects the shape of the blade, which is the angle between the absolute motion direction and the normal direction of the cutting edge [7]. The larger the sliding–cutting angle is, the smaller the cutting force, but a sliding–cutting angle that is too large is not conducive to stable clamping, so its value ranges from 20° to 30°. The oblique angle is the edge angle of the cutter. If the oblique angle is too small, the service life of the cutter is reduced, and if it is too large, the cutting resistance is increased. In this paper, the oblique angle of the cutter ranges from 35° to 45° [6]. The average cutting speed is the ratio of a single cutting displacement to the reciprocating movement time of the cutter. It is an important indicator to measure the cutting performance. Some studies have found that when the cutting speed is too fast, the cutting resistance increases, obviously, and when the cutting speed is too small, the cutting motion becomes difficult [20]. Therefore, the average

cutting speed was set at 300 to 500 mm/s. The test was divided into 20 groups, and the coding table of test factor levels is shown in Table 3.

**Table 3.** Levels and codes of experimental variables.

| Level | Test Factors | | |
|---|---|---|---|
| | Sliding–Cutting Angle $X_1$ (°) | Oblique Angle $X_2$ (°) | Average Cutting Speed $X_3$ (mm/s) |
| −1.682 | 16.59 | 31.59 | 231.82 |
| −1 | 20 | 35 | 300 |
| 0 | 25 | 40 | 400 |
| 1 | 30 | 45 | 500 |
| 1.682 | 33.41 | 48.41 | 568.18 |

### *2.4. Experiment and Methods*

In order to verify the accuracy of the numerical simulation results and detect the cutting effect under the best parameters of the reciprocating cutting system, the cutting performance experiment was carried out.

The Chinese little greens variety used were Nanjing Yongxin, with a growth cycle of 35 days. The average height of the selected Chinese little greens selected in the experiments was 180 ± 30 mm, the length of the cutting position was 10 ± 3 mm, and the diameter of the stalk was 7 ± 2 mm. Before the cutting test, five Chinese little greens roots were randomly weighed and recorded. They were then dried continuously in an oven for 24 h (ASABE standard, 2012). The equation for calculating moisture content follows:

$$M = \frac{M_L}{M_W} \times 100\% \tag{3}$$

where $M$ is the moisture content, %; $M_L$ is the weight lost, g; and $M_W$ is the sample weight, g.

The leaves of the root were removed, and the whole plant was transplanted into a seedling tray and fixed. The test sample is shown in Figure 5a. A reciprocating cutting stress measurement system for the Chinese little greens was built [34]. The test system was mainly composed of a stalk-feeding device, a cutting device, and a cutting stress measurement system. The specific working parameters of the test bench are shown in Table 4.

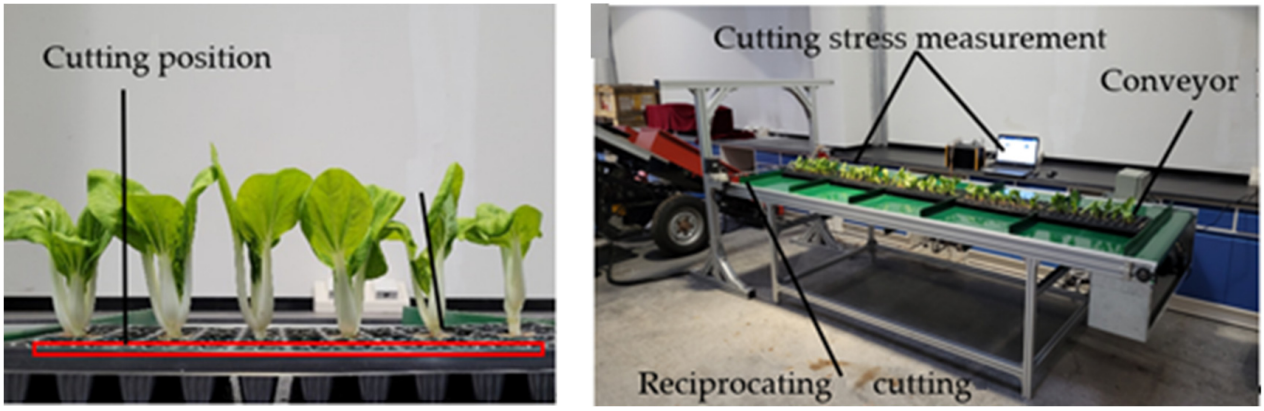


(**a**) (**b**)

**Figure 5.** Schematic diagram of measurement system of cutting stress: (**a**) test sample; (**b**) cutting stress measurement system.

**Table 4.** Parameters of the reciprocating cutting test system.

| Parameters | Values |
|---|---|
| Average cutting speed/mm·s$^{-1}$ | 0~1500 |
| Reciprocating cutting stroke/mm | 30 |
| Average feeding speed/mm·s$^{-1}$ | 0~1000 |
| Resistance strain measurement range/Mpa | 0~100 |
| Resistance strain gauge sensitivity factor | 2.17 ± 1% |
| Data collection frequency/Hz | 500 |
| Data acquisition channel | 1~4 |

The stalk-feeding device includes a frequency converter, an AC motor, a conveyor belt, and a stalk-fixing seedling tray. The stalk-fixing tray of greens was placed on the center of the conveyor belt, which was powered by an AC motor to drive the seedling tray forward. The frequency converter was used to adjust the feeding speed of the stems, and the specific structure is shown in Figure 6a. The cutting device was fixed on the frame by fastening bolts, including a controller, a DC motor, a cutter, a transmission device, and a frame. In operation, the double eccentric wheel mechanism was driven by the stepping motor. The phase difference between the two eccentric wheels was transmitted to the eccentric shaft through the reduction gear, thereby driving the upper and bottom blades to make a reciprocating linear motion. The average cutting speed can be adjusted by the DC motor, and its structure is shown in Figure 6b. The test system mainly includes a resistance strain gauge and a DH5902N solid data acquisition system. A set of adjacent blades for each of the upper and bottom blades was selected, and the surface of the blades was polished and cleaned. A set of strain gauges at the center of the blades was installed in rectangular distribution, so that the principal stresses of the blades in the *X* and *Y* directions were collected. The *X* direction was in line with the cutting direction, and the *Y* direction was in line with the stalk-feeding direction. The strain gauge was connected to the data acquisition system through wiring. It sends the mechanical signals of the cutter to the dynamic signal acquisition and analysis system for real-time data recording of stress data. The specific structure is shown in Figure 6c.

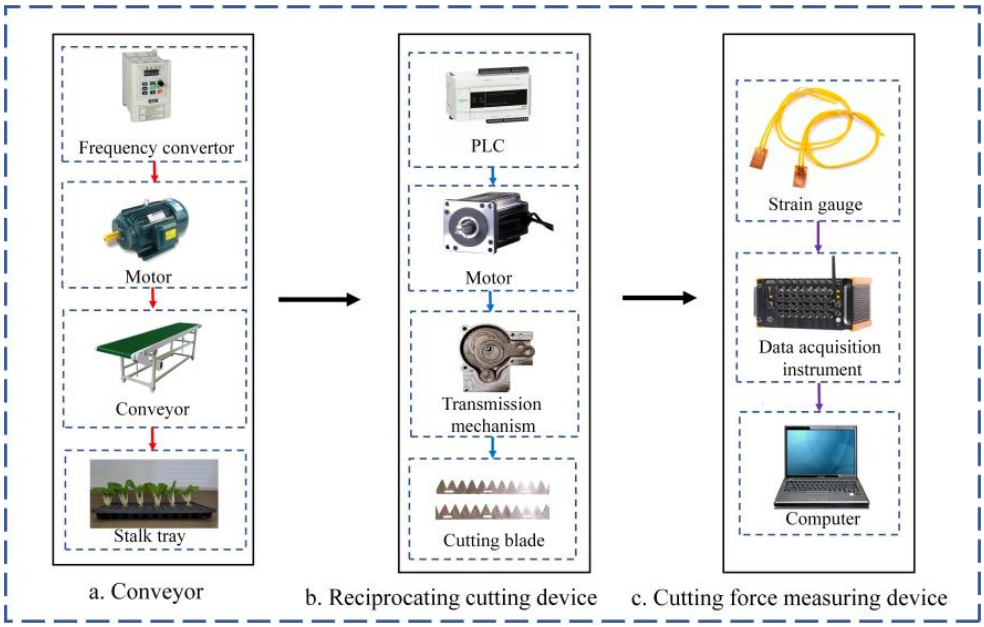


**Figure 6.** Structural diagram of the cutting force measurement system.

Before the test, stalks with a diameter of 5 mm were selected, and the leaf crown on the top of the parsley was constructed and fixed on the conveying device. By adjusting the

distance between the cutting blade and the conveying device by adjusting the fastening bolt between the blade holder and the frame, the appropriate cutting position was determined. In the test, start the test system and motor, and adjust the frequency converter to adjust the control frequency, and keep the stalk-feeding speed at a constant value of 200 mm/s. The structural parameters of the cutting blade were kept unchanged, but the frequency operation of the cutting motor was adjusted by controller to obtain different average cutting speeds. After the various systems of the test bench enter stable operation, the motor of the conveying device was started [34]. The installation and wiring diagram of the resistance strain gauge sensor is shown in Figure 7. The sensor collected four sets of data for the cutting normal stress of the upper and bottom blades in real time, and then the data were transmitted to the PC terminal after being processed by the dynamic data acquisition system. Considering that the maximum cutting stress was an influencing factor that affects cutting power consumption and effect, the maximum cutting stress was taken as the test result. Each test was repeated three times, and the average value of the ultimate cutting stress was taken as the reference value and compared with the results of numerical simulation [24].

(**a**) (**b**) (**c**)

**Figure 7.** Schematic diagram of arrangement and wiring of strain gauge: (**a**) installation locations of the strain gauges on the upper blade; (**b**) installation locations of strain gauges on the bottom blade; (**c**) wire connection between the data acquisition instrument and computer.

## 3. Results

### *3.1. Post-Processing Results and Analysis of Numerical Simulation*

After calculating the numerical simulation, the calculation results underwent post-processing [23]. The equivalent stress distribution cloud diagram was obtained in the cutting process when the sliding–cutting angle was 20°, the oblique angle was 35°, and the average cutting speed was 300 mm/s. Figure 8 reflects the dynamic change in equivalent stress during the cutting process. It can be seen from Figure 8a that when t is 0 ms, the cutting blade and the stalk were out of touch, and the equivalent stress between the cutting blade and the greens was 0 Mpa. Then the cutting blade moved toward the stalk at 300 mm/s, and contacted the stalk at 25.9 ms. Figure 8b (t = 26.8 ms) shows the cloud map of the equivalent stress distribution at the initial cutting stage. The cutting blade compressed the stalk locally to produce significant buckling and plastic deformation, and the fiber tensile stress continued to increase, and the shear strain exceeded the tensile strength of the fibers. Hence, the unit was damaged and failed, the fibers of the stalk broke at the blade edge, and then the cutter gradually cut into the stalk. At this time, both the upper and bottom cutting blades had stress concentration, and the maximum equivalent stresses appeared at the contact point on the stalk, which were 0.31 and 0.68 Mpa, respectively. The sheared part of the stalk showed the maximum equivalent stress, which was 3.93 Mpa, which was consistent with the actual working conditions. As shown in Figure 8c (t = 30.3 ms), at the stage of stalk rupture, when the blade cut into about one-half the diameter of the stalk, and the stem tissues at the tip of the blade were further bent and deformed, which eventually caused the entire fiber layer to slip and break, resulting in shear damage to the entire stem. At this stage, stress concentration occurred throughout

the cutting edge. The reason might be that the stalk exerted greater squeezing and friction on the cutter at a deeper position. At this time, the cutting cross section had a tendency to crack, and the surface of the stubble of the cracked part was uneven with poor quality. Therefore, the relevant cutting parameters should be optimized to reduce this phenomenon. Figure 8d reflects the process of separating stalks from the stubbles after the cutting was completed. During this process, the stalks were cut and separated. The stress concentration of the cutting blade and the stalks gradually disappeared, then reaching the minimum. The effect force was significantly reduced, but the cutter still had residual stress.

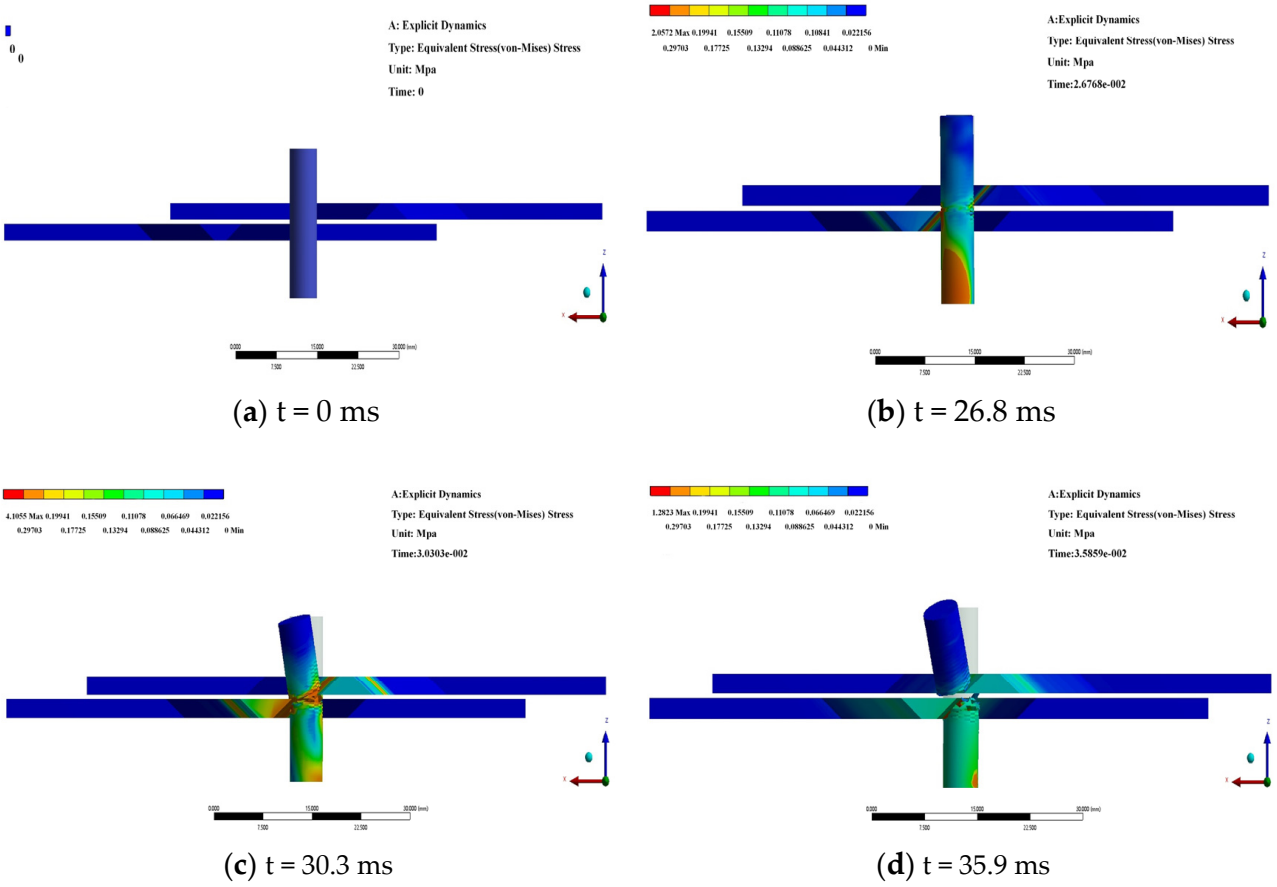


(**a**) t = 0 ms (**b**) t = 26.8 ms

(**c**) t = 30.3 ms (**d**) t = 35.9 ms

**Figure 8.** The effective stress cloud diagram of cutting unit.

The equivalent stress curves are shown in Figure 9. It can be seen that the cutting blade and the stalk contacted each other at about 26 ms, and the cutting operation was completed at about t = 36 ms. The entire cutting process lasted about 10 ms, during which the cutting equivalent stress of the process continued to change dynamically, which was consistent with the actual working conditions of the shearing process. There was no interaction between the cutter and the stalk after separation; however, since the cutter was still affected by the residual stress, the stress of the cutter at this stage was not zero. When t = 28.1 ms, the maximum equivalent stress of the upper cutting blade was 1.05 Mpa. The maximum equivalent stress of the lower cutting blade occurred at t = 36.6 ms, which was 0.90 Mpa. The maximum equivalent stress of the cutting blade is much lower than 355 Mpa, which is the tool material yield limit. It means that the cutter would not undergo significant plastic deformation.

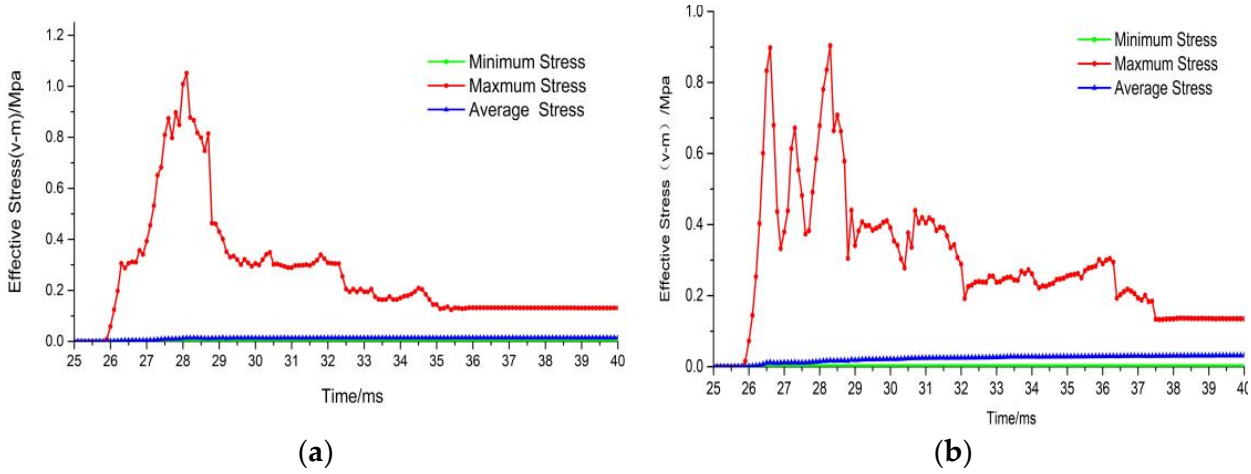


(**a**) (**b**)

**Figure 9.** Equivalent stress curves of cutting blade: (**a**) upper cutting blade; (**b**) bottom cutting blade.

Figure 10 shows cloud diagrams for the maximum equivalent stress distribution of the cutting blade during the cutting process. Taking the description of Figure 10a as an example, it can be seen that area A, where the upper cutting blade contacts the stalk, received the greatest reaction stress, and here was the peak value of local stress. In addition, the stress mainly occurred in the edge area of the cutting blade, which showed that the method and position of the strain gauges used in this study were reasonable.

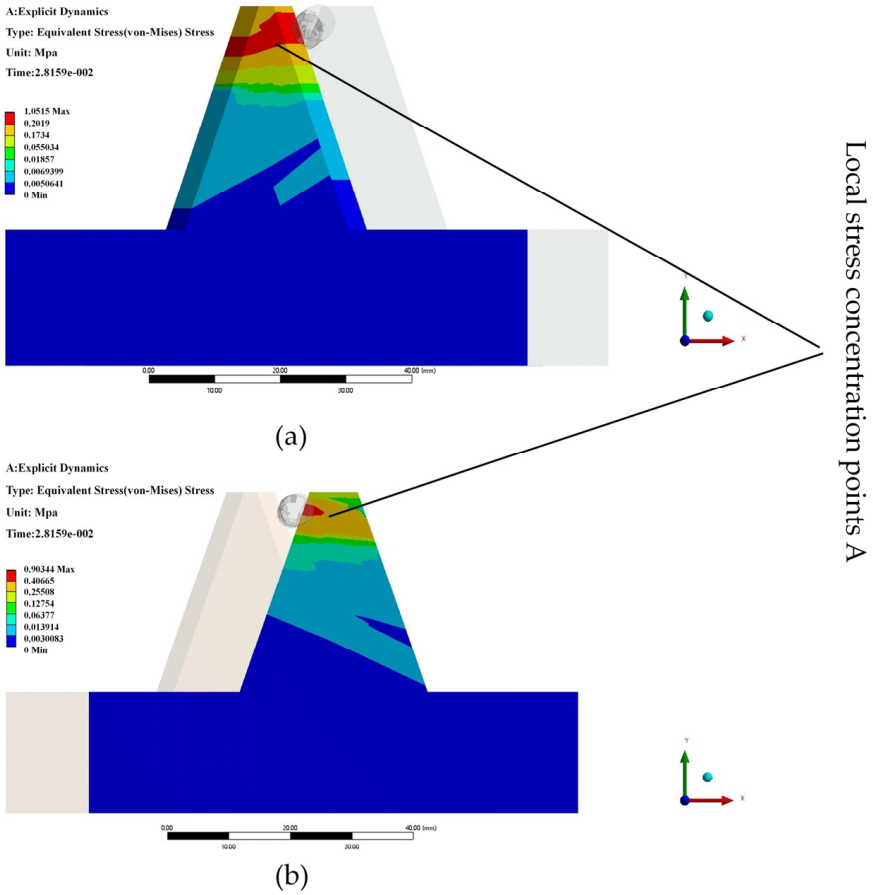


**Figure 10.** Maximum equivalent stress distribution cloud diagram: (**a**) upper cutting blade; (**b**) bottom cutting blade.

### 3.2. Orthogonal Test Results and Significance Analysis

According to the test method described in Section 2.2, the numerical simulation of the cutting orthogonal test was carried out using Design-Expert 10.0.7 software. A total of 20 sets of simulation tests were performed; the test results are shown in Table 5.

**Table 5.** Design and results of the orthogonal test in numerical simulation.

| Test Number | Test Factors | | | Test Indicators | |
|---|---|---|---|---|---|
| | $X_1$ ($\alpha$) ° | $X_2$ ($\beta$) ° | $X_3$ ($V$) mm/s | $Y_1$ ($\sigma_1$) Mpa | $Y_2$ ($\sigma_2$) Mpa |
| 1 | 0.000 | 0.000 | 0.000 | 1.06 | 0.83 |
| 2 | −1.000 | −1.000 | 1.000 | 1.11 | 1.02 |
| 3 | −1.000 | 1.000 | −1.000 | 1.58 | 1.65 |
| 4 | 0.000 | 0.000 | 0.000 | 1.07 | 0.92 |
| 5 | 1.000 | 1.000 | 1.000 | 1.19 | 1.10 |
| 6 | 1.000 | −1.000 | 1.000 | 0.90 | 0.81 |
| 7 | 0.000 | 0.000 | 0.000 | 1.26 | 0.72 |
| 8 | −1.000 | 1.000 | 1.000 | 1.48 | 1.60 |
| 9 | 1.000 | −1.000 | −1.000 | 1.17 | 1.17 |
| 10 | 0.000 | 1.682 | 0.000 | 1.62 | 1.74 |
| 11 | 0.000 | −1.682 | 0.000 | 1.25 | 1.17 |
| 12 | −1.682 | 0.000 | 0.000 | 1.34 | 1.31 |
| 13 | 0.000 | 0.000 | −1.682 | 1.20 | 1.10 |
| 14 | 0.000 | 0.000 | 0.000 | 1.10 | 0.96 |
| 15 | −1.000 | −1.000 | −1.000 | 1.05 | 0.90 |
| 16 | 1.000 | 1.000 | −1.000 | 1.24 | 1.17 |
| 17 | 0.000 | 0.000 | 0.000 | 1.08 | 0.95 |
| 18 | 0.000 | 0.000 | 0.000 | 1.07 | 0.92 |
| 19 | 1.682 | 0.000 | 0.000 | 1.12 | 1.10 |
| 20 | 0.000 | 0.000 | 1.682 | 0.99 | 0.82 |

The test results were analyzed by multiple regression fitting using Design-Expert 10.0.7 software, and the regression equation between maximum cutting equivalent stresses and each influencing factor were established. The insignificant terms were then removed. Regression equations are shown in Equations (4) and (5):

$$Y_1 = 1.11 - 0.08X_1 + 0.14X_2 - 0.052X_3 - 0.067X_1X_2 + 0.11X_{22} \quad (4)$$

$$Y_2 = 0.88 - 0.093X_1 + 0.19X_2 - 0.061X_3 - 0.13X_1X_2 + 0.10X_{12} + 0.19X_{22} \quad (5)$$

The variance analysis of the regression equation is shown in Tables 6 and 7. According to the variance analysis of the maximum cutting equivalent stresses $Y_1$ and $Y_2$ of the cutter, it can be seen that the significance level $p$ values of the two models were both less than 0.01, indicating that the models were extremely significant. The values for the lack-of-fit items of the regression model were all greater than 0.05, indicating that the regression model had a high fitting accuracy. The coefficients of determination $R^2$ for the two models were 90.4% and 93.9%, respectively, indicating 90.4% and 93.9% of the total variation in the limit cutting force can be explained by this model, so that both models had high reliability [35–37]. Therefore, the structural and working parameters of the reciprocating cutting system can be optimized and analyzed by models.

It can be seen from the results of the variance analysis that various factors had different effects on the indicators. The $p$ value reflected the degree of influence for each parameter of the regression equation. The smaller $p$ value had more significant effect. The oblique angle had the greatest influence, followed by the sliding–cutting angle and average cutting speed, and these three factors were significant items ($p < 0.05$).

**Table 6.** Variance analysis results for $Y_1$.

| Source | Sum of Squares | Freedom | Mean Square | *F*-Value | *p*-Value |
|---|---|---|---|---|---|
| Model | 0.61 | 9 | 0.068 | 10.48 | 0.0005 |
| $X_1$ | 0.087 | 1 | 0.087 | 13.43 | 0.0044 |
| $X_2$ | 0.26 | 1 | 0.26 | 40.04 | <0.0001 |
| $X_3$ | 0.037 | 1 | 0.037 | 5.75 | 0.0375 |
| $X_1X_2$ | 0.036 | 1 | 0.036 | 5.63 | 0.0392 |
| $X_1X_3$ | 0.0098 | 1 | 0.0098 | 1.51 | 0.2469 |
| $X_2X_3$ | 0.00045 | 1 | 0.00045 | 0.069 | 0.7975 |
| $X_1^2$ | 0.016 | 1 | 0.016 | 2.52 | 0.1437 |
| $X_2^2$ | 0.16 | 1 | 0.16 | 25.05 | 0.0005 |
| $X_3^2$ | 0.0028 | 1 | 0.0028 | 0.44 | 0.5214 |
| Residual | 0.065 | 10 | 0.0064 | | |
| Lack of Fit | 0.036 | 5 | 0.0071 | 1.22 | 0.4149 |
| Pure Error | 0.029 | 5 | 0.0058 | | |
| Cor. Total | 0.68 | 19 | | | |

**Table 7.** Variance analysis results for $Y_2$.

| Source | Sum of Squares | Freedom | Mean Square | *F*-Value | *p*-Value |
|---|---|---|---|---|---|
| Model | 1.46 | 9 | 0.16 | 17.18 | <0.0001 |
| $X_1$ | 0.12 | 1 | 0.12 | 12.56 | 0.0053 |
| $X_2$ | 0.49 | 1 | 0.49 | 51.53 | <0.0001 |
| $X_3$ | 0.051 | 1 | 0.051 | 5.35 | 0.0433 |
| $X_1X_2$ | 0.14 | 1 | 0.14 | 14.31 | 0.0036 |
| $X_1X_3$ | 0.031 | 1 | 0.031 | 3.31 | 0.0990 |
| $X_2X_3$ | 0.0018 | 1 | 0.0018 | 0.19 | 0.6718 |
| $X_1^2$ | 0.15 | 1 | 0.15 | 16.36 | 0.0023 |
| $X_2^2$ | 0.53 | 1 | 0.53 | 56.20 | <0.0001 |
| $X_3^2$ | 0.0041 | 1 | 0.0041 | 0.44 | 0.5227 |
| Residual | 0.094 | 10 | 0.00093 | | |
| Lack of Fit | 0.052 | 5 | 0.010 | 1.21 | 0.4207 |
| Pure Error | 0.043 | 5 | 0.0086 | | |
| Cor. Total | 1.56 | 19 | | | |

According to Tables 6 and 7, it can be seen that the interaction terms of factor $X_1$ and $X_2$ had a significant impact on the two indicators ($p < 0.05$), and the three-dimensional response surface of the two-factor interaction effect are shown in Figures 11 and 12 [38,39]. The change rate of the test index for the upper cutter and bottom cutter along the factor $X_2$ direction was faster than that along the factor $X_1$ direction. At the same time, as the sliding–cutting angle increased, the cutting resistance on the cutter gradually decreased. The reason is that the cutting has a sliding progression during the cutting process. The larger sliding–cutting angle of the cutter can make more tangential slip. When the oblique angle of the cutter was 35~38°, the stress on the cutter gradually decreased, and then when the oblique angle continued to increase, the stress on the cutting knife gradually increased. It can be seen from the contour map that the rate of change in the test index along the factor $X_2$ direction is faster than for the factor $X_1$, which means that the oblique angle has a more significant influence on the cutting stress than the sliding angle.

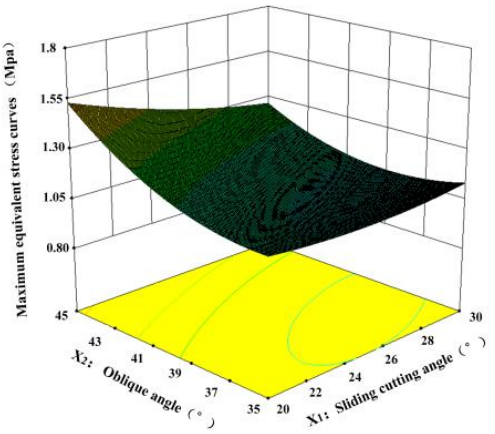


**Figure 11.** Effects of the sliding–cutting angle and the oblique angle on maximum equivalent stress of the upper cutting blade.

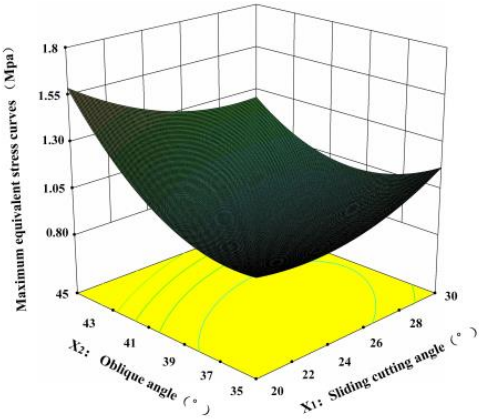


**Figure 12.** Effects of the sliding–cutting angle and the oblique angle on maximum equivalent stress of the bottom cutting blade.

### *3.3. Regression Model Optimization*

In order to optimize the working parameters of the reciprocating cutting system, the maximum cutting stress of the upper cutter and the bottom cutter were set as the optimal object, and the optimization model was established as follows:

$$\begin{cases} f = minY_1 \\ f = minY_2 \\ \begin{cases} 20^\circ \le X_1 \le 30^\circ \\ 35^\circ \le X_2 \le 45^\circ \\ 300\ \text{mm/s} \le X_3 \le 500\ \text{mm/s} \end{cases} \end{cases} \quad (6)$$

The model was optimized by using Design-Expert 10.0.7 software's data optimization module, Optimization and the optimal cutting parameter combination for the reciprocating cutting system of greens was obtained: sliding–cutting angle was 29°, oblique angle was 38°, and average cutting speed was 500 mm/s. The maximum equivalent stress in cutting of the upper cutter and the bottom cutter is the minimum value, and their predicted values are 0.95 and 0.77 Mpa, respectively.

### *3.4. Analysis of Cutting Performance Test Results*

The root moisture calculated by Equation (3) was 88.7% ± 2.1%, and the difference in moisture content between samples was small, indicating that the root moisture content had little effect on the test results. In order to verify the accuracy of the numerical simulation

results and the actual cutting effect, the cutting performance test was carried out according to the equipment and methods described in Section 2.4.

The resistance strain gauge collected normal stress of both blades and obtained four sets of data. Figure 13 shows the maximum normal cutting stress results when the sliding–cutting angle is 29°, the oblique angle is 38°, and the average cutting speed is 300, 400, and 500 mm/s. In three sets of physical tests, the maximum cutting stress in the *X* direction of each group is less than the maximum cutting stress in the Y direction, which is consistent with the numerical simulation results. As the average cutting speed decreases, the maximum cutting stress shows an increasing trend, and the test index is the minimum when the average cutting speed is 500 mm/s. The physical test verifies the reliability of the test platform. The parameters of the Chinese little greens cutting device were optimized.

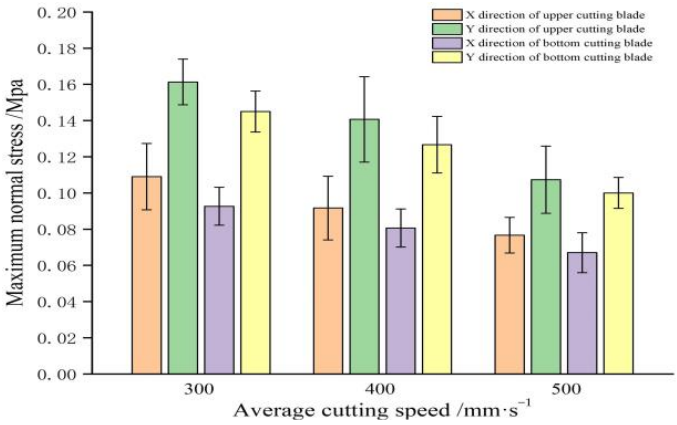


**Figure 13.** Maximum normal cutting stress at different average cutting speeds used in the physical tests.

## 4. Discussion

The cutting mechanical properties of the stalks of Chinese little greens were investigated by numerical simulation technology, and then the optimal cutting combination parameters were obtained. Finally, the simulation results were verified to be sensitive and reliable by physical experiments. The results of this study showed that the sliding–cutting angle, oblique angle, and the average cutting speed all had a significant effect on the maximum cutting stress, and the optimal cutting combination parameters were 29°, 38°, and 500 m/s, respectively. Results indicated that dynamic simulation techniques are simple and effective compared to traditional physical testing methods.

We found that the oblique edge angle had the most significant effect on the maximum cutting stress, reaching the optimum value at 38°. When the oblique angle was 35~38°, the cutting stress was proportional to the oblique angle. This is because the squeezing and rubbing effect of the stalk fibers on the cutter become stronger when the blades are gradually cut into the stalk, and the resistance of the cutting blade to destroy the stalk fibers increases, so stress concentration is prone to occur. Furthermore, the cutting stress was inversely proportional to sliding angle. This result is comparable to the results of the study by Cui et al. [6] and Zhang et al. [7], which proved that the stalk of Chinese little greens has similar cutting mechanical properties to that of lettuce and rice. However, a sliding angle that is too large will cause problems such as unstable clamping and cutting failure. The cutting stress is smaller for high-speed cutting progress, and it was in agreement with millet stalk [40]. In addition, the cutting power consumption was proportional to the cutting speed in some studies [15,18]. This result may be due to the inconsistent physical properties of apple tree branches and greens. It also may be because the cutting-stress speed curve is a U-shaped curve. When cutting progresses at low speed, the cutting blades generate impact kinetic energy, and the impact force at the moment of contact with the stalk will cause the fiber structure to rupture and reduce the cutting resistance. When a certain threshold is reached, however, the cutting stress increases with the increase in cutting speed.

However, it is worth noting that the explicit dynamic analysis technology still has certain limitations, such as an inability to realize the simulation of continuous and reciprocating cutting progress, which has a certain error with the actual operating conditions. In addition, mechanical vibration during cutting also affects simulation accuracy. Considering the short harvest period for vegetables and the cultivation mode of facility agriculture, the effect of constitutive parameters among plant materials, such as differences in moisture content on cutting resistance, was also not considered in this study. Further studies would help to optimize cutting parameters according to material constitutive parameters.

## 5. Conclusions

A simulation model of the cutting system for Chinese little greens was established, and the influence law of the working parameters of the cutting device on cutting characteristics was studied. The optimal cutting parameters were obtained by using the method of combining numerical simulation and orthogonal experiment. The result showed that significant influence on the maximum cutting stress was related, in decreasing order, to the oblique angle, the sliding–cutting angle, and the average cutting speed. The ultimate cutting equivalent stress of the upper cutting blade was 0.95 Mpa, and that of the bottom cutter was 0.77 Mpa, at the condition of optimal parameter combinations. Physical tests of stalk cutting showed that the test index was the smallest under the optimal parameter combination. The optimal parameter combination of the cutter in tests significantly reduces the cutting resistance, which provides a reference for the optimization of the cutting device for the Chinese little greens.

**Author Contributions:** Conceptualization, Z.Y. and W.W.; methodology, X.L. and W.W.; software, W.W.; formal analysis, W.W.; investigation, Z.Y.; writing—original draft preparation, X.L.; writing—review and editing, W.W.; supervision, W.W.; funding acquisition, X.L. All authors have read and agreed to the published version of the manuscript.

**Funding:** This research was supported by the Jiangsu Agricultural Science and Technology Innovation Fund (No. CX (19)2025) and the Jiangsu Modern Agricultural Equipment and Technology Demonstration Promotion Fund (No. NJ2020–23).

**Institutional Review Board Statement:** Not applicable.

**Informed Consent Statement:** Not applicable.

**Data Availability Statement:** Not applicable.

**Conflicts of Interest:** The authors declare no conflict of interest.

## References

1. Liu, D.; Xiao, H.R.; Yang, G.; Jin, Y.; Yang, G.; Cao, G.Q.; Zhang, J.F.; Liu, M. Design and experiment of the orderly harvester of Chinese little greens. *Int. Agric. Eng. J.* **2018**, *27*, 295–306.
2. Shah, D.U.; Reynolds, T.P.S.; Ramage, M.H. The strength of plants: Theory and experimental methods to measure the mechanical properties of stems. *J. Exp. Bot.* **2017**, *68*, 4497–4516. [CrossRef] [PubMed]
3. Zhou, D.; Jing, C.; She, J.; She, J.K.; Tong, J.; Chen, Y.X. Temporal dynamics of shearing force of rice stem. *Biomass Bioenergy* **2012**, *47*, 109–114. [CrossRef]
4. Wang, Y.; Yang, Y.; Zhao, H.M.; Liu, B.; Ma, J.T.; He, Y.; Zhang, Y.T.; Xu, H.B. Effects of cutting parameters on cutting of citrus fruit stems. *Biosyst. Eng.* **2020**, *193*, 1–11. [CrossRef]
5. Gan, H.; Mathanker, S.; Momin, M.A.; Kuhns, B.; Stoffel, N.; Hansen, A.; Grift, T. Effects of three cutting blade designs on energy consumption during mowing-conditioning of Miscanthus Giganteus. *Biomass Bioenergy* **2018**, *109*, 166–171. [CrossRef]
6. Cui, Y.J.; Wang, W.Q.; Wang, M.H.; Ma, Y.D.; Fu, L.S. Effects of cutter parameters on shearing stress for lettuce harvesting using a specially developed fixture. *Int. J. Agric. Biol. Eng.* **2021**, *14*, 152–158. [CrossRef]
7. Zhang, C.L.; Chen, L.Q.; Xia, J.F.; Zhang, J.M. Effects of blade sliding cutting angle and stem level on cutting energy of rice stems. *Int. J. Agric. Biol. Eng.* **2019**, *12*, 75–81. [CrossRef]
8. Esgici, R.; Pekitkan, F.G.; Ozdemir, G. Cutting parameters of some grape varieties subject to the diameter and age of canes. *Fresenius Environ. Bull.* **2019**, *28*, 167–170.
9. Du, D.D.; Wang, J.; Qiu, S.S. Analysis and test of splitting failure in the cutting process of cabbage root. *Int. J. Agric. Biol. Eng.* **2015**, *8*, 27–34.

10. Boyda, M.G.; Omakli, M.; Sayinci, B.; Kara, M. Effects of moisture content, internode region, and oblique angle on the mechanical properties of sainfoin stem. *Turk. J. Agric. For.* **2019**, *43*, 254–263. [CrossRef]
11. Clementson, C.L.; Hansen, A.C. Pilot study of manual sugarcane harvesting using biomechanical analysis. *J. Agric. Saf. Health* **2008**, *14*, 309–320. [CrossRef] [PubMed]
12. Vu, V.D.; Ngo, Q.H.; Nguyen, T.T.; Nguyen, H.C.; Nguyen, Q.T.; Nguyen, V.D. Multi-objective optimization of cutting force and cutting power in chopping agricultural residues. *Biosyst. Eng.* **2020**, *191*, 107–115. [CrossRef]
13. Ma, P.B.; Li, L.Q.; Wen, B.Q.; Xue, Y.H.; Kan, Z.; Li, J.B. Design and parameter optimization of spiral-dragon type straw chopping test rig. *Int. J. Agric. Biol. Eng.* **2020**, *13*, 47–56. [CrossRef]
14. Cheng, S.; Zhang, B.; Li, X.W.; Yin, G.D.; Chen, Q.M.; Xia, C.H. Bench cutting tests and analysis for harvesting hemp stalk. *Int. J. Agric. Biol. Eng.* **2017**, *10*, 56–67. [CrossRef]
15. Johnson, P.C.; Clementson, C.L.; Mathanker, S.K.; Grift, T.E.; Hansen, A.C. Cutting energy characteristics of Miscanthus x giganteus stems with varying oblique angle and cutting speed. *Biosyst. Eng.* **2012**, *112*, 42–48. [CrossRef]
16. Mathanker, S.K.; Grift, T.E.; Hansen, A.C. Effect of blade oblique angle and cutting speed on cutting energy for energy cane stems. *Biosyst. Eng.* **2015**, *133*, 64–70. [CrossRef]
17. Allameh, A.; Alirzadeh, M.R. Specific cutting energy variations under different rice stem cultivars and blade parameters. *Idesia* **2016**, *34*, 11–17. [CrossRef]
18. Zhao, J.L.; Huang, D.Y.; Jia, H.L.; Zhuang, J.; Guo, M.Z. Analysis and experiment on cutting performances of high-stubble maize stalks. *Int. J. Agric. Biol. Eng.* **2017**, *10*, 40–52.
19. Stopa, R.; Komarnicki, P.; Kuta, Ł.; Szyjewicza, D.; Słupska, M. Modeling with the finite element method the influence of shaped elements of loading components on the surface pressure distribution of carrot roots. *Comput. Electron. Agric.* **2019**, *167*, 105046. [CrossRef]
20. Meng, Y.; Wei, J.D.; Wei, J.; Chen, H.; Cui, Y.S. An ANSYS/LS-DYNA simulation and experimental study of circular saw blade cutting system of mulberry cutting machine. *Comput. Electron. Agric.* **2019**, *157*, 38–48. [CrossRef]
21. Yang, W.; Yang, J.; Liu, Z.H.; Liang, Z.X.; Mo, J.L. Dynamic simulation experiment of one-blade cutting sugarcane process. *Trans. Chin. Soc. Agric. Mach.* **2011**, *27*, 150–156.
22. Huang, H.D.; Wang, Y.X.; Tang, Y.Q.; Zhao, F.; Kong, X.F. Finite element simulation of sugarcane cutting. *Trans. Chin. Soc. Agric. Eng.* **2011**, *27*, 161–166.
23. Qiu, M.M.; Meng, Y.M.; Li, Y.Z.; Shen, X.B. Sugarcane stem cut quality investigated by finite element simulation and experiment. *Biosyst. Eng.* **2021**, *206*, 135–149. [CrossRef]
24. Xie, L.X.; Wang, J.; Cheng, S.M.; Zeng, B.S.; Yang, Z.Z. Optimisation and finite element simulation of the chopping process for chopper sugarcane harvesting. *Biosyst. Eng.* **2018**, *175*, 16–26. [CrossRef]
25. Luo, Y.Q.; Ren, Y.H.; Zhou, Z.X.; Huang, X.M.; Song, T.J. Prediction of single-tooth sawing force based on tooth profile parameters. *Int. J. Adv. Manuf. Technol.* **2016**, *86*, 641–650. [CrossRef]
26. Liu, Q.; Mathanker, S.K.; Zhang, Q.; Hansen, A.C. Biomechanical properties of miscanthus stems. *Trans. Asabe* **2012**, *55*, 1125–1131. [CrossRef]
27. Maughan, J.D.; Mathanker, S.K.; Grift, T.; Hansen, A.C. Impact of Blade Angle on Miscanthus Harvesting Energy Requirement. In Proceedings of the 2013 Kansas City, Kansas City, MI, USA, 21–24 July 2013.
28. Moiceanu, G.; Voicu, P.; Paraschiv, G.; Voicu, G. Behaviour of miscanthus at cutting shear with straight knives with different edge angles. *Environ. Eng. Manag. J.* **2017**, *16*, 1203–1209. [CrossRef]
29. Yang, W.; Zhao, W.J.; Liu, Y.D.; Chen, Y.Q.; Yang, J. Simulation of forces acting on the cutter blade surfaces and root system of sugarcane using FEM and SPH coupled method. *Comput. Electron. Agric.* **2020**, *180*, 105893. [CrossRef]
30. Liu, D.; Xiao, H.R.; Jin, Y.; Cao, G.Q.; Shen, C.; Yang, G.; Zhang, J.F.; Liu, M. Mechanical properties test and analysis on the stalks of Chinese little greens. *Int. Agric. Eng. J.* **2018**, *27*, 38–43.
31. Salarikia, A.; Ashtiani, S.M.; Golzarian, M.R.; Mohammadinezhad, H. Finite element analysis of the dynamic behavior of pear under impact loading. *Inf. Process. Agric.* **2017**, *4*, 64–77. [CrossRef]
32. Ahmadi, E.; Barikloo, H.; Kashfi, M. Viscoelastic finite element analysis of the dynamic behavior of apple under impact loading with regard to its different layers. *Comput. Electron. Agric.* **2016**, *121*, 1–11. [CrossRef]
33. Hasanzadeh, R.; Mojaver, M.; Azdast, T.; Park, C.B. Polyethylene waste gasification syngas analysis and multi-objective optimization using central composite design for simultaneous minimization of required heat and maximization of exergy efficiency. *Energy Convers. Manag.* **2021**, *247*, 114713. [CrossRef]
34. Zhao, J.; Guo, M.Z.; Lu, Y.; Huang, D.Y.; Zhuang, J. Design of bionic locust mouthparts stubble cutting device. *Int. J. Agric. Biol. Eng.* **2020**, *13*, 20–28. [CrossRef]
35. Xie, L.X.; Wang, J.; Cheng, S.M.; Zeng, B.S.; Yang, Z.Z. Optimisation and dynamic simulation of a conveying and top breaking system for whole-stalk sugarcane harvesters. *Biosyst. Eng.* **2020**, *197*, 156–169. [CrossRef]
36. Hu, H.N.; Li, H.W.; Wang, Q.J.; He, J.; Lu, C.Y.; Wang, Y.B.; Wang, C.L. Performance of waterjet on cutting maize stalks: A preliminary investigation. *Int. J. Agric. Biol. Eng.* **2019**, *12*, 64–70. [CrossRef]
37. Wang, J.; Yang, W.; Sun, X.; Li, X.; Tang, H. Design and experiment of spray and rotary tillage combined disinfection machine for soil. *Int. J. Agric. Biol. Eng.* **2019**, *12*, 52–58. [CrossRef]

38. Hu, H.N.; Li, H.W.; Wang, Q.J.; He, J.; Lu, C.Y.; Wang, Y.B.; Liu, P. Anti-blocking performance of ultrahigh-pressure waterjet assisted furrow opener for no-till seeder. *Int. J. Agric. Biol. Eng.* **2020**, *13*, 64–70. [CrossRef]
39. Huang, J.; Tian, K.; Shen, C.; Zhang, B.; Liu, H.L.; Chen, Q.M.; Li, X.W.; Ji, A. Design and parameters optimization for cutting-conveying mechanism of ramie combine harvester. *Int. J. Agric. Biol. Eng.* **2020**, *13*, 94–103. [CrossRef]
40. Zhang, Y.Q.; Cui, Q.L.; Guo, Y.M.; Li, H.B. Experiment and analysis of cutting mechanical properties of millet stem. *Trans. Chin. Soc. Agric. Mach.* **2019**, *50*, 146–155.